Research Square

Preprints are preliminary reports that have not undergone peer review.
They should not be considered conclusive, used to inform clinical practice,
or referenced by the media as validated information.

Drug-free in vitro activation combined 3D-bioprinted adipose-derived stem cells restore ovarian function of premature ovarian insufficiency

Qian Li
The Second Hospital of Hebei Medical University
Jiahua Zheng
The Second Hospital of Hebei Medical University
Zhongkang Li
The Second Hospital of Hebei Medical University
Yanlai Xiao
The Second Hospital of Hebei Medical University
Mingle Zhang
The Second Hospital of Hebei Medical University
Wenxin Shi
The Second Hospital of Hebei Medical University
He Gao
The Second Hospital of Hebei Medical University
Xianghua Huang (huangxh2003@163.com)
Second Hospital of Hebei Medical University https://orcid.org/0000-0002-4609-1222
Jingkun Zhang
The Second Hospital of Hebei Medical University

Research Article

Keywords: Drug-free in vitro activation, 3D-bioprinting, Adipose-derived stem cells, Decellularized extracellular matrix, Premature ovarian insufficiency, Vascularization, PI3K/AKT signaling pathway

Posted Date: May 18th, 2022

DOI: https://doi.org/10.21203/rs.3.rs-1634227/v1

License: This work is licensed under a Creative Commons Attribution 4.0 International License.
Read Full License

Abstract

Background

Emerging drug-free in vitro activation (IVA) technique enables patients with premature ovarian insufficiency (POI) to restore ovarian function and conceive their own genetic offspring. However, many issues have greatly restricted its clinical application. Mesenchymal stem cells (MSCs) could significantly stimulate neovascularization and increase blood perfusion to reduce the loss of primordial follicles, and effectively improve the quality and number of oocytes in aged mice. Here, we designed a 3D-bioprinted engineering ovary composed of drug-free IVA and adipose-derived stem cells (ADSCs), which may prolong the retention of ADSCs and construct an early vascular microenvironment, thus compensating for the disadvantages of drug-free IVA to some extent and ameliorating impaired ovarian function in the POI rats.

Methods

After intraperitoneal injection of cyclophosphamide, the POI model rats were randomized into 5 groups: (1)POI group; (2)ovarian fragments group; (3)3D scaffold combined with ovarian fragments group; (4)ovarian fragments combined with ADSCs group; (5)3D scaffold with ADSCs combined with ovarian fragments as 3D-bioprinted engineering ovary group. Normal rats were identified as the control group. The localization of CM-Dil labeled ADSCs and co-localization with CD31 were observed to examine the distribution and underlying mechanism of differentiation. Histomorphological and immunohistochemical analyses were performed to enumerate follicle number and assess granulosa cells (GCs) proliferation and apoptosis. Immunofluorescence staining was used to evaluate angiogenesis. Hormone levels were measured to evaluate the restoration of endocrine axis. Western blot analysis and RT-PCR were conducted to explore the potential mechanism.

Results

CM-Dil-labeled ADSCs were distributed in the interstitium of ovaries and had significantly higher retention in the 3D-bioprinted engineering ovary group. Some regions of the CM-Dil (+) staining co-expressed with CD31 staining were in the area of vascular endothelial cells. Meanwhile, the follicle counts, GCs proliferation and apoptosis, neoangiogenesis and hormone levels were significantly improved in the 3D-bioprinted engineering ovary group, as compared with other groups. Furthermore, the ovarian function was ameliorated and angiogenesis was promoted through regulating the PI3K/AKT pathway.

Conclusion

Our results suggested that 3D-bioprinted engineering ovary had great potential for restoring impaired ovarian function of POI, which could compensate for the disadvantages of drug-free IVA to some extent.

Background

Premature ovarian insufficiency (POI) that occurs in 1% of women younger than 40 years would be the ultimately clinical performance of accelerated ovarian follicular exhaustion, for which the only option is egg donation [1]. Despite dormant residual follicles in several POI patients, they are less likely to grow after traditional treatment and difficult to fertilize with their own eggs. In vitro activation (IVA) of dormant residual follicles is emerging as a novel effective approach for restoring fertility to women with POI, which enable them to conceive their own genetic offspring [2, 3]. The approach is established based on the ovarian fragmentation of resting follicles activated by Hippo signaling pathway and manipulation of the phosphatase and tensin homolog (PTEN)/phosphatidylinositol-3-kinase(PI3K)/protein kinase B(AKT)/forkhead box O3(FOXO3) pathway to activating primordial follicles [2, 3]. However, due to the low rate of pregnancy and potential carcinogenic effects of pharmacologic approaches, a simplified drug-free IVA method to promote follicle growth by disrupting Hippo signaling pathway alone was put forward [4, 5]. To date, several success pregnancies and live births have been reported from the IVA of ovarian tissues [6–12]. Compared with conventional IVA, a number of researchers have assumed that the drug-free activation seemed to be more efficient [13]. Despite ample evidence that supports the effectiveness of drug-free IVA with respect to the rate of clinical pregnancy and birth rate, there are still numerous issues that have greatly restricted its application, such as low pregnancy rates, loss of substantial number of primordial follicles, and unimproved quality of age-associated oocytes [2, 13].

To our knowledge, ischemic injury from delayed revascularization between ovarian tissues and recipients is a major cause of premature follicle depletion and low survival of graft [14]. Therefore, the future studies should concentrate on promoting early post-transplantation revascularization and improving fertility associated with age-related declines in oocyte quality. Numerous studies have demonstrated that mesenchymal stem cells (MSCs) could significantly stimulate neovascularization and increase blood perfusion to reduce the loss of primordial follicles [15, 16], and effectively improve the quality and number of oocytes in aged mice [17–19], thus representing a new strategy toward boosting fertility in women with reduced ovarian reserve. Although MSCs have shown potency in recovering ovarian function and enhancing fertility, quick diffusion and insufficient retention are the major restrictions for the application of MSCs therapy [20]. Consequently, various types of scaffolds encapsulating MSCs have been applied to increase both short- and long-term retention to further enhance the efficiency of MSCs [21, 22].

Decellularized extracellular matrix (dECM), derived from natural tissues, has been treated to maximally remove cellular and antigenic components to minimize immune response, while preserving the natural skeleton of ECM [23]. The dECM-based scaffold recreates excellent in vivo ovarian microenvironment, ensuring the MSCs and ovarian cell viability, facilitating the cells for necessary interaction with their surrounding environment [24], and also supporting the viability and function of in vitro cultured ovarian

cortical tissues [25]. Therefore, we focused on utilizing 3D-bioprinted scaffold based on ovarian dECM-based “bioinks” encapsulating adipose-derived stem cells (ADSCs), supporting more cell retention and survival in the target tissue, as well as exhibiting a powerful pro-angiogenesis effect, which in turn reduce ischemic injury of the follicles.

Given the potential role of the early revascular microenvironment constructed by 3D-bioprinted ovarian scaffold, as well as IVA of dormant residual follicles, we hypothesized that the combination of aforementioned two approaches could be applied to minimize ischemic injury of ovarian tissue through enhancing early angiogenesis and blood oxygen supply, thus restoring ovarian function. Based on the above hypothesis, our research was designed for a novel 3D-bioprinted engineering ovary and assessing the effect of the above system on the revascularization in the grafts and restoration of ovarian function in the POI rats.

Methods

ADSCs culture and characterization

The isolation and cultivation of ADSCs was performed according to previously publicized protocol [26]. ADSCs were cultured in serum-free basic MSC medium (Beijing Jing-Meng Cell Biological Technology Co., Ltd., China) supplemented with serum-free nutritional substance, and 1% penicillin/streptomycin (Gibco, USA) in a humidified incubator with 5% carbon dioxide at 37℃. After approximately every 48 h the culture medium was changed and passaged until cells reached 90% confluence.

The specific surface-antigens of ADSCs (Passage 3–5) such as CD45, CD90, CD105, CD29, CD73, CD44 and HLA-DR (Biosciences, USA) were identified by Flow cytometry (FCM). The multi-potency of ADSCs was verified by osteogenic and adipogenic differentiation following the manufacture’s protocol. In brief, ADSCs of 90% confluence were co-incubated with adipogenic induction medium and osteogenic induction medium (Gibco, USA) for up to 14 or 28 d and induced cells were detected by Oil Red O and Alizarin red (Sigma, USA) respectively.

Acquisition, decellularization and histological analysis of porcine ovarian tissue

Porcine ovaries was harvested from a local abattoir (Shijiazhuang, China) from 6-month-old pigs and transferred to the laboratory in precooling saline. Upon arrival at the laboratory, according to the process we described previously [27], redundant unwanted tissues and ovary medulla were removed. The ovarian cortex was cut into 500 um small fusiform strips, after being rinsed multiple times with water to remove excess plasma, all samples were decellularized, lyophilized and stored in -20℃ refrigerator. Individual native and decellularized porcine ovarian tissue samples were fixed in 4% paraformaldedyde for 24–48 h at room temperature, followed by hematoxylin and eosin (HE) staining, Masson staining and 4’6-Diamidino-2-Phenylindole (DAPI; Southern Biotech, China) staining.

3D “bioinks” preparation and 3D printing

3D “bioinks” preparation was performed as previously described [28]. Briefly, lyophilized dECMs were grinded into powder with the assistance of liquid N2. 100 milligram (mg) of dECM powder, and 60 mg of pepsin (porcine, Sigma, USA) was dissolved in 3 ml of concentrated hydrochloric acid (pH = 2.0), mixed well with a small spoon and shaken at 37℃ and 80 × g for 22–24 h. When the primary glue was completely digested, the pH value of dECM solution was re-adjusted to 7.35–7.45 by 10M NaOH addition to deactivate pepsin and stop digestion. The mixture of 300 mg of gelatin (Sigma, USA) and 60 mg of sodium alginate (Sigma, USA) in 2 ml tri-distilled water was performed at 55℃ for 30 min, then mixed with pH 7.35–7.45 dECM solution to create dECM “bioinks”. Terminal dECM “bioinks” disinfection was circulated three rounds of 56℃ and 4℃ for 15min each time.

The liquid dECM “bioinks” mixed thoroughly with/without above cultured ADSCs ($1x10^7$cells mL^{-1}) were loaded into the top of barrel and then placed at 4℃ for 15min to cool the hydrogel into a gel. Using a 3D-Printer (Bio-Architect®-WS; Hangzhou Regenovo Biotechnology, Ltd.,China), dECM “bioinks” was printed from a 340um stainless steel cooling sprinkler (set at 20℃) onto a platform controlled at 4℃. The extrusion pressure was set according to the ink flow velocity (≈ range from 0.18 to 0.32 kPa), and 3D scaffolds (8×8×3 mm^3, a circular porous grid scaffold) were printed at a scanning speed of $6mms^{-1}$. Immediately after printing, the formed structures were cross-linked for 5min with 5% calcium chloride solution and then washed with sterilized phosphate-buffered saline (PBS; Servicebio, China) for three times. Scaffolds were then incubated overnight in fresh medium at 37℃ incubator containing 5% CO2.

Preparation of POI rat model and experimental treatment groups

All animal experiments in this study were performed according to the Ethics Committee of Second Hospital of Hebei Medical University (2021-AE055). Female Sprague-Dawley rats (8–10 weeks old) were provided by Experimental Animal Center of Hebei Medical University (Shijiazhuang, China) for in vivo experiments. The animal models of POI (8–10 weeks old) were induced by daily intraperitoneal injection of cyclophosphamide (CTX; Sigma, USA) (50mg/kg on the first day and 8mg/kg/day for the following 14 consecutive days) [29], while the rats in the control group were intraperitoneally administered equivalent volumes of saline. We evaluated the successful establishment of POI model by performing pathological analysis of the obtained ovaries, monitoring vaginal smears and measuring body weight every day for two weeks after CTX injection.

The experimental treatment groups were treated through 1 cm bilateral micro-incisions on the lower back, and the ovaries were removed from the top of the uterine horns. The surrounding tissues of collected whole ovaries were carefully separated, and ovarian cortex was cut into fragments of $1×1×1mm^3$. The scaffold-fragment/3D-bioprinted engineering ovary was established using 3D scaffold (with or without cells) and POI ovarian fragments by wrapping of the latter into 3D stent strut (schematic representation is shown in Fig. 2A). Then blunt subcutaneous separations were carried out above the dorsal incision to

form two tunnels, the scaffold-fragment/3D-bioprinted engineering ovary/ovarian fragments (with or without cells) were placed at both sides of the back, and then each incision was sutured in an interrupted fashion with 4 – 0 absorbable sutures (Shanghai Pudong Jinhuan Medical Products Co., LTD), separately.

Intervention of POI rats with subcutaneous implantation of the grafts

The animals that underwent surgical procedure were always in the diestrus phase. Sixty POI rats with disrupted estrous cycle and weight reduction were enrolled and randomized into five groups as follows (n = 12, each group): (1)untreated group as POI group; (2)subcutaneous transplantation of ovarian fragments ($1\times1\times1mm^3$) alone group as fragment-alone group; (3)subcutaneous 3D scaffold ($8\times8\times3mm^3$) without cells combined with ovarian fragments group as scaffold-fragment group; (4)subcutaneous ovarian fragments combined with ADSCs (6×10^6 ADSCs in 60ul PBS per entire rat) group as fragment-cell group; (5)subcutaneous 3D scaffold with ADSCs (1×10^7 ADSCs in 100ul PBS mixed with 1ml of “bioinks”, 0.6ml “bioinks” per entire rat) combined with ovarian fragments group as 3D-bioprinted engineering ovary group. Twelve normal rats without any treatment were identified as the control group. Then the samples were collected from four rats in each group after sacrifice at 1, 2, and 4 weeks after treatment for subsequent experiments.

Tracking of transplanted ADSCs in grafts

To track the localization of transplanted ADSCs, approximately 1×10^6 ADSCs were added with 1 ml of culture medium containing 2 mg CM-Dil (Thermo, USA) at 37°C for 10 min and 4°C for 20 min. Subsequently, the labeled cells were rinsed twice with sterile PBS to remove the unbound CM-Dil, and suspended in PBS for subcutaneous transplantation with ovarian fragments (6×10^6 cells per rat) or thoroughly well-mixed with “bioinks” (1×10^7 cells ml^{-1} “bioinks”, 0.6ml “bioinks” per entire rat) for printing. The bilateral grafts were removed at 1 and 4 weeks after transplantation, fixed with optimal cutting temperature (OCT) compound and cut into 6 um in thickness using a cryostat (Leica, Germany), incubated with DAPI and subsequently imaged under a fluorescence microscope (Olympus, Japan) to examine the survival and distribution of ADSCs in vivo.

Assessment of ovarian function

a) Ovarian morphological analysis and follicle counts

The grafts from all the experimental groups were collected at 1, 2 and 4 weeks after transplantation, fixed in 4% paraformaldehyde, then dehydrated in a gradient ethanol followed by xylene vitrification, paraffin-embedment, and sectioning into 5μm serial sections. The ovarian morphology was recognized by HE staining and visualized using optical microscope (Zeiss, Germany). We calculated varying stages of follicles (primordial, primary, secondary and antral follicles) in different sections of each group as we had

characterized previously [30]. Only those containing a visual oocyte were calculated to avoid overcounting follicles.

b) Immunohistochemistry staining and TUNEL analysis

To observe the effects of ovarian follicle proliferation and apoptosis in each group after treatment, the sections were immune stained with proliferation marker anti-Ki67 (1:800, Servicebio, China) and apoptosis marker anti-caspase-3 antibody (1:800, Servicebio, China) overnight at 4℃, followed by biotinylated secondary antibody (ZSGB-Bio, China) for 1 h and staining using DAB staining solution (ZSGB-Bio, China). Nuclei were co-stained with hematoxylin. The statistical analysis of Ki67-positive and Casepase-3-positive areas was evaluated from four randomly selected regions of discontinuous three sections of each sample. In addition, a TUNEL assay kit (Servicebio, China) was used to further evaluate the apoptosis of representative areas in each group at 4 weeks after transplantation. The procedure was performed following the manufacturer's introductions. The green staining cells were apoptotic cells while DAPI (blue) staining was nuclei.

c) Immunofluorescence (IF) staining

Newly formed endothelial surface marker CD31 and proliferating cell nuclear antigen (PCNA) were detected by IF to assess angiogenesis and proliferation of the grafts. Briefly, the sections were blocked in a solution of 0.2% TritonX-100 containing 3% goat serum for 1.5 h and incubated with anti-CD31 antibody (1:800, Servicebio, China), and anti-PCNA antibody (1:800, Servicebio, China) in antibody dilutions overnight at 4℃ followed by incubation with fluorescently labeled corresponding secondary antibody (1:400, Servicebio, China) at 37℃ for 1.5 h, and then DAPI was routinely used to counterstain nuclei. The number of CD31-labled neovascularization from each sample was calculated based on the five randomly selected regions of three discontinuous sections. Furthermore, we applied double-staining with CM-Dil and CD31 to analyze the differentiation of ADSCs in 3D-bioprinted engineering ovary group, and the fresh frozen sections were obtained from the samples at 4 weeks after transplantation. The specific staining method was performed as described previously. Fluorescent images were acquired using an optical microscope (Zeiss, Germany).

d) Hormone assay

At the specified time point of the study (at 1, 2, 4 weeks after transplantation), blood samples were collected from eyeball of the rats in the dioestrus and stored overnight at 4℃, and then serum was obtained and frozen at -80℃ for further analysis. Enzyme-linked immunosorbent assay (ELISA) was employed in the measurement of Estradiol (E2), follicle stimulating hormone (FSH) and antimüllerian hormone (AMH) according to the manufacturer's instructions (Cloud-Clone, China). The concentrations of hormone were calculated using standard curves.

Western blot analysis and real-time PCR (RT-PCR)

Total protein was extracted from ovarian tissues with RIPA lysis buffer (Servicebio, China) supplemented with proteinase inhibitors and phosphatase inhibitors (Servicebio, China). The normalized concentration of proteins was denatured and isolated using 10% SDS-PAGE (Biotides, China), and then transferred to PVDF membranes (Millipore, USA). The membranes were blocked for 1.5 h with 5% bovine serum albumin (BSA; Sigma, USA) (in TBS + 0.1% Tween-20, PH = 7.4), followed by incubation with appropriate primary antibodies as follows: VEGF (1:2000, Zen-bioscience, China), total AKT (1:2000, Zen-bioscience, China), p-Akt (1:1000, Zen-bioscience, China), PI3K (1:1000, Zen-bioscience, China) and GAPDH (1:4000, servicebio, China) at 4°C overnight. Afterwards, the membranes were washed three times and incubated with M5 Goat Anti-Rabbit IgG-HRP (1:10000, Mei5bio, China) at room temperature for 1 h. Lastly, the protein bands were visualized using the ChemiDoc MP Imaging System (Bio-Rad, USA) and analyzed using Image J software.

Expression levels of angiogenesis-associated mRNA (FGF2, angiogenin and VEGF) were then quantified by RT-PCR (primers sequences were listed in Table 1). Total RNA was extracted from ovarian tissues using TRIzol Reagent (Servicebio, China) and reverse transcribed into complementary DNA (cDNA) using the RevertAid First Strand cDNA Synthesis Kit (Thermo, USA). RT-PCR was performed using MonAmp™ ChemoHs qPCR Mix (Monad, China) and the final analysis results were calculated according to $2^{-\Delta\Delta Ct}$ method.

Statistical analysis

Statistical analyses of all results were performed using GraphPad Prism 6.0 and SPSS 26.0 software and the data are expressed as the mean ± SD. F-test was used to assess the homogeneity of variances. A Student t-test, One-way ANOVA and Mann–Whitney U-test were performed to evaluate the difference between groups. Statistical significance was considered at P values < 0.05.

Table1 Primers used for RT-PCR validation

Gene	Primer FW	Primer RW
VEGF	GCTTTACTGCTGTACCTCCACCATG	CATCTCTCCTATGTGCTGGCTTTGG
Angiogenin	TGGCAACAAGGGCAGCATCAAG	ACTCATCAAAGTGGACAGGCAAGC
FGF-2	CATCACTTCGCTTCCCGCACTG	GCAGCCGTCCATCTTCCTTCATAG
GAPDH	GTCCATGCCATCACTGCCACTC	CGCCTGCTTCACCACCTTCTTG

Results

Characterization of ADSCs

ADSCs at the third to five passage showed morphologically uniform, adherent, fibroblast-like long spindles. Flow cytometry indicated that the ADSCs were enriched with MSCs's surface markers CD29 (97.25%), CD73 (90.25%), CD105 (98.09%), CD44 (99.63%), and CD90 (99.66%), but few were positively expressed with CD45 (0.24%) and HLA-DR (0.69%). Furthermore, these cells possessed multi-potent characteristics of adipocytes and osteoblasts through in vitro induction, which were concordant with our previous research on ADSCs [31] (Supplementary data, Fig. S1A-C).

Decellularization of porcine ovarian tissue

We chose porcine ovarian ECM to create a fully functioning engineered ovary because a range of physical and chemical process ensured removal of cellular constituents while sustaining the overall structure and components to support restoration of specific tissue structure and functional recovery [32, 33]. To evaluate the validity of decellularization, we conducted histological assays in the native and decellularizad tissues. Consequently, we utilized HE staining and DAPI staining to confirm the preservation of native ECM materials and the absence of cellular components. Then, Masson staining results confirmed that the collagen was well sustained in the ECM (Supplementary data, Fig. S2A). All these results showed that dECM preserved overall structure and composition of native tissue, thereby serving as 3D-bioprinted "bioink" in guiding cell anchorage, growth and migration.

Evaluation of the established POI model

In our study, we observed that body weights of POI group began to drop in the first week after medication, with a marked decline in the second week which was significantly lower than in the normal group. Compared with the regular estrous cycle in the normal group, the POI group had a longer diestrus and irregular estrous cycle. In addition, pathological staining revealed that the number of follicles at all levels was remarkably reduced, and TUNEL staining of apoptotic GCs were obviously increased in the POI group (Supplementary data, Fig. S2B-D). These results indicated that we had successful created a rat model of chemotherapy-induced POI.

In vivo tracking of ADSCs

In the present study, we aimed to trace the in vivo localization of CM-Dil-labeled ADSCs with or without 3D printing scaffold after transplantation and the underlying mechanism- of-differentiation. After labeling, the cell membrane had a homogeneously distributed red fluorescence and did not show obvious decline in cell passage (Fig. 1A). Furthermore, we traced the fate of CM-Dil-marked ADSCs in the frozen section of grafts at 1 week and 4 week after transplantation. As shown in Fig. 1B, the red fluorescence signals were distributed in the interstitium of ovaries transplanted with CM-Dil-ADSCs or scaffold/ADSCs rather than in follicles. With time, the fluorescence signals progressively reduced either in ADSCs or scaffold/ADSCs, but the higher retention ratio of scaffold/ADSCs was detected at 1 week and 4 week after transplantation. In addition, the positive staining for CD31 was green, the co-expressed site of red, blue, and green were white. We observed that some regions of the CM-Dil(+) staining co-expressed with CD31 staining were in the area of vascular endothelial cells (Fig. 1C). These results indicated that 3D printing dECM scaffold

supported survival, growth, and proliferation of ADSCs and was helpful in promoting retention of ADSCs, and that a fraction of ADSCs might have differentiated into vascular endothelial cells.

Construction and transplantation of 3D-bioprinted engineering ovary

The mechanical properties, 3D printability, biocompatibility and comparable cytocompatibility of dECM "bioink" had been demonstrated by our previous research [28]. The purpose of our study was to create a 3D-bioprinted engineering ovary. Thus, we queried whether the overall ovarian cortex fragments could be inserted while maintaining the 3D scaffold structure and integrity. Figure 2B showed that the fragments were totally inserted into the scaffold and the system remained polyporous and macroscopically intact. Grafts of each group were successfully transplanted into the subcutaneous pockets of the POI rats and completely removed without any complications. At 2 and 4 weeks after transplantation, the recovered ovarian fragments with/without ADSCs were found to be rejoined, integrated, and wrapped by a hyaline membrane and adherent to the subcutis (Fig. 2C). The constructs of 3D scaffold combined with ovarian fragments (with or without ADSCs) could maintain their structure, but had a slight degradation with the prolongation of time (Fig. 2C). All grafts were surrounded by visible functional blood vessels, but grafts from the fragment-alone/3D scaffold group had less vascularization and more pale appearance than those from other two containing ADSCs groups. Moreover, macroscopically the 3D-bioprinted engineering ovary grafts had more surrounding blood vessels than other groups, and preovulatory follicles were found in the grafts (Fig. 2C).

Ovarian morphological analysis and follicle counting

The initial experiments of our study were to investigate the biocompatibility between ovarian tissue and 3D scaffold, since the ambient suitable conditions were influencing factors for internal nutrient supply of ovarian tissue and follicle survival. We explored appropriate stent size and construction, and found that 3D scaffold ($8\times8\times3mm^3$) could serve as proper microenvironment for survival of ovarian fragments. Figure 3A exhibited that any stage of healthy-looking follicles survived and developed within the dECM scaffold with/without ADSCs and did not provoke a marked pathologic response.

Subsequent studies explored the therapeutic effects of containing ADSCs groups on the restoration of ovarian function. Histological staining of retrieved implants revealed that the number of any stage of follicles in POI group degenerated markedly relative to normal group (Fig. 3B). In the fragment-alone group and scaffold-fragment group, the number of growing follicles increased while no remarkable increase was found in the primordial follicles (Fig. 3B). More excitingly, the pool of primordial follicles and growing follicles was variously increased in fragment-cell group and 3D-bioprinted engineering ovary group (Fig. 3B).

We further quantified the number of follicles in different groups to evaluate the therapeutic effects (Fig. 3C). In the first two weeks after transplantation, although the number of primordial follicles and primary follicles in the fragment-alone group and scaffold-fragment group were no significantly different

compared with the POI group, the number of secondary and antral follicles increased to some extent (P< 0.05). At four weeks after transplantation, the number of primordial follicles (P< 0.05), primary follicles (P< 0.05), secondary follicles (P< 0.05), and antral follicles (P< 0.05) in the above two groups were higher than that in the POI group, but still significantly lower than that in the containing ADSCs groups (P< 0.05). Based on comparisons of POI group and the other two treatment groups, there were markedly increased percentage of each stage of follicles observed from the two weeks after transplantation in the fragment-cell group and 3D-bioprinted engineering ovary group (P< 0.05), and reached normal or near-normal range after four weeks (P< 0.05), but no significant difference was reported between the two groups. Overall, these data indicated that the effects of ovarian fragmentation combined with ADSCs on the increase in ovarian reserve and reduction in ovarian injury in the POI rats.

Estrous cycle and hormone levels

We detected the estrous cycle and serum hormone levels of E2, AMH, and FSH to investigate the therapeutic effects of grafts transplantation on restoration of ovarian function in POI rats. Our finding demonstrated that the proportion of irregular estrous cycles after chemotherapy was decreased from the second week in the four treatment groups. At the end of the fourth week, 75%(3/4) of rats in fragment-cell group and 3D-bioprinted engineering ovary group had regular estrous cycle, which were significantly higher compared to POI group and the other two treatment groups (Fig. 3E). The ELISA results indicated that the levels of FSH and AMH were slightly recovered in the four treatment groups relative to the POI group starting with the first week, especially the fragment-cell group and 3D-bioprinted engineering ovary group. By contrast, the recovery of E2 that started in the second week after transplantation and gradually increased with prolonged recovery. However, at the end of the fourth week, the levels of E2 and AMH in 3D-bioprinted engineering ovary group were significantly higher than those in other treatment groups and near-normal level (Fig. 3D, P < 0.05). In addition, the level of FSH was decreased to the normal level at four weeks after treatment in 3D-bioprinted engineering ovary group and differed markedly from the other treatment groups (Fig. 3D, P < 0.05). These findings confirmed that all of the treatment groups could upgrade serum hormone levels and restore ovarian function, which was most pronounced in fragment-cell group and 3D-bioprinted engineering ovary group, especially the latter one.

Proliferation and angiogenesis

Ki67 and PCNA (molecular proliferation marker) were investigated, and caspase-3 and TUNEL staining (molecular apoptosis marker) were performed to further estimate the proliferation and apoptosis of GCs of follicles at different stages in the grafted tissues. As shown in our results, there were more positive Ki67 follicles in the fragment-cell group and 3D-bioprinted engineering ovary group compared with other treatment groups at 1, 2, and 4 weeks post-transplantation, especially the 3D-bioprinted engineering ovary group at 4 weeks post-transplantation, which was similar to that of the normal group (Fig. 4A/E, P< 0.05). Similarly, our results indicated that PCNA showed more positive proliferative GCs in the fragment-cell group and 3D-bioprinted engineering ovary group, which were higher than those in the other groups by IF staining (Fig. 4C). Furthermore, we evaluated the apoptosis of follicles in different groups using caspase-3 and TUNEL staining at 4 weeks after transplantation. The caspase-3 immunostaining showed that the

apoptosis of follicles decreased significantly in four treatment groups — fragment-alone group, scaffold-fragment group, the fragment-cell group and 3D-bioprinted engineering ovary group — compared to the POI group, the disparities was most pronounced in 3D-bioprinted engineering ovary group (Fig. 4B/F, $P < 0.05$). The same result was also confirmed by the TUNEL staining (Fig. 4D).

Our above results had confirmed more retention of ADSCs in the 3D-bioprinted engineering ovary group. Therefore, we further evaluated whether more ADSCs encapsulation affected the incidence and degree of local dECM neovascularization, which had direct effects on the follicle survival and longevity of the grafts. By IF analysis, we detected higher CD31-positive signals and functioning blood vessels in the 3D-bioprinted engineering ovary group, as compared with the other groups (Fig. 5A). Additionally, a larger number of positively stained cells by CD31 was found at 1 week post-transplantation and also increased significantly at 4 weeks, indicating the continuous vascular remodeling (Fig. 5B, $P < 0.05$). In the fragment-cell group, although there was neovascular infiltration at 1 week post-transplantation, the vascularization was not maintained and significantly decreased at 4 weeks post-transplantation ($P < 0.05$). In the fragment-alone group and scaffold-fragment group, we also detected neovascularization at 1 week and 4 weeks post-transplantation, but the number of vessels was significantly less than that of the other two groups ($P < 0.05$).

Activation of the PI3K/AKT pathway to promote angiogenesis

To gain further understanding of the mechanism of containing ADSCs groups promoting the angiogenesis of the grafts, the expression of proangiogenesis-related proteins related to PI3K/Akt signal pathway was detected. Compared with POI group, higher p-AKT, PI3K expression and VEGF upregulation were detected in the fragment-cell group and 3D-bioprinted engineering ovary group (Fig. 6A/B, $P < 0.05$), while the levels of total AKT did not significantly differ from the other two groups (Fig. 6A/B, $P > 0.05$). Moreover, although the expression levels of the above proteins in 3D-bioprinted engineering ovary group were higher than those in the fragment-cell group, there was no significant difference in the expression of p-AKT and PI3K (Fig. 6A/B, $P > 0.05$) except VEGF (Fig. 6A/B, $P < 0.05$). As recognized by the mRNA expression of VEGF, FGF-2 and angiogenin, there was a significant upregulation in containing ADSCs groups compared with the POI group and the other two treatment groups, especially the 3D-bioprinted engineering ovary group (Fig. 6C, $P < 0.05$). Taken together, these findings suggested the role of ADSCs in promoting angiogenesis by activating the PI3K/AKT pathway.

Discussion

In our study, we designed for the first time a novel 3D-bioprinted engineering ovary, which combined ovarian fragments with 3D printing scaffold employing dECM-derived “bioink” containing ADSCs, to restore impaired ovarian function in POI. The results of our study demonstrated that 3D scaffold not only prolonged the retention of ADSCs, but also increased blood flow accompanied by the prolonged blood perfusion at one week after transplantation, which would decrease post-transplantation hypoxia-ischemia

and improve follicle survival. Next, our study further demonstrated that the 3D-bioprinted engineering ovary, compared with other treatment groups, increased production of follicles at various stages, showing a significantly faster recovery of hormone levels and estrous cycle, increased proliferation and reduced apoptosis of ovarian cells. Finally, we substantiated that our therapeutic mechanism of POI involved facilitating angiogenesis by regulating the PI3K/AKT pathway.

In recent years, IVA is a rapidly advancing method of activating and regulating follicle growth developed by Kawamura et al. [3]and Suzuki et al. [10]. The conventional IVA is a two-step process that first requires in-vitro culture of ovarian with PTEN inhibitor or PI3K activator for two days to activate dormant primordial follicles, followed by the second step of ovarian cortical fragmentation to activate follicule growth by suppressing Hippo signaling pathway [2, 3]. This approach has been successfully applied to patients with POI, which enabled them to conceive with their own genome. However, this technique has been hampered by secondary surgical trauma, low rate of pregnancy and potential carcinogenic effect of pharmacologic substances [4, 5]. Thus, a less invasive method of drug-free IVA has been developed to promote follicle growth by disrupting Hippo signaling alone (mechanical stimulation alone). To date, despite several success pregnancies and live birth that have been reported from the IVA of ovarian tissue in POI, various issues have greatly restricted its application, such as the loss of substantial number of primordial follicles, unimproved quality of age-associated oocyte, and poor therapeutic success [2, 13]. Similarly, our study also observed an increased number of growing follicles and hormonal levels in the fragment-alone group and scaffold-fragment group, however, the reduced primordial follicle pool and limited therapeutic effects require further optimization.

It’s well known that the number of residual follicles and disease duration are the major determinant of therapeutic success of IVA [11], and early post-transplantation hypoxia is one of the major negative issues affecting the survival of follicles [34]. Therefore, we should attempt to improve ovarian reserve and promote early revascularization to improve follicle survival [35, 36]. Currently, numerous studies have shown that MSCs have the therapeutic effects on the restoration of ovarian function and fertility in POI by homing to injured site, differentiating into GCs or oocytes [37, 38], and secreting multiple bioactive substances through paracrine mechanism [29, 39]. A number of studies have reported the angiogenic potential of ADSCs [40] and pre- constructed a prepared vascularized grafting region via ADSCs to promote ovarian cell survival [41, 42]. In addition, the application of exosomes derived from human umbilical mesenchymal stem cells (HucMSC-exos) not only improved ovarian reserve by effectively stimulating primordial follicles, but also rescued the oocyte production and quality of age-related decline in fertility [43]. For the above stated reasons, we combined the two therapeutic methods together and observed that the fragment-cell group had early revascularization of grafts, restoration of hormone levels and continuously increasing proportion of growing follicles as well as a high percentage of primordial follicles during the 4 weeks after transplantation. This demonstrated a protective effect of ADSCs on ovarian reserve and follicular activation of ovarian fragmentation, which was considered to be responsible for faster recovery of ovarian function. However, we traced the distribution of CM-Dil-labeled ADSCs and found they were mainly located in the interstitial tissue of impaired ovary, and the fluorescence signals significantly reduced with prolonged time after transplantation. Additionally,

although we observed the revascularization of grafts within 1 week, the vascularization was not maintained and significantly decreased at 4 weeks. The therapeutic effects were weakend due to their quickly diffusion [20, 44] and low viability of retained cells in the target tissue [45].

Recently, the application of regenerative medicine biomaterials, such as collagen, hydrogel and fibrin, are a promising approach to delivery and maintenance of seeding cells in the target organ [21, 22, 46, 47]. However, these biomaterials are less able to fully simulate the complex extracellular ecological environment for survival of various cell [48]. Thus, enormous endeavors have been devoted to the application of dECM, since they support a variety of cells due to their complex tissue-specific properties and unique composition of functional components [49, 50], thus providing excellent biochemical functionality and biocompatibility [51] for tissue remodeling and function recovering [33, 52]. Our previous studies demonstrated that our dECM had maximized removal of cells while preserving the structure and composition of native tissue [27, 28]. In addition, we also successfully designed a 3D printing scaffold employing dECM “bioink” encapsulating bone marrow mesenchymal stem cells (BMSCs), which demonstrated a promising approach to vagina reconstruction [28]. To our knowledge, the obtained 3D scaffold recreated in vitro the complexity of in vivo native tissue milieu, overcoming the disadvantages of 2D culture system (i.e. loss of tissue-specific architecture and changes in cellular morphology and function) and providing the structural support between the cell culture environment and the surrounding tissue environment [25]. In addition, the 3D scaffold not only improved cell retention, proliferation and differentiation, but also promoted angiogenesis, nutrient supply and functional recovery by loading more cells [27, 28]. Therefore, we engineered a novel 3D-bioprinted engineering ovary composed of 3D scaffold containing ADSCs and ovarian cortical fragments. Our results confirmed that 3D scaffold could provide ADSCs into an appropirate niche and thus increase the retention and survival of ADSCs during a long period, while the ADSCs alone experienced significant cells loss within 4 weeks after transplantation. With more loading of ADSCs into 3D scaffold, accompanied by an increased secretion of soluble growth factors (VEGF, FGF2, and angiogenin) [22], the number of blood vessels was significantly increased as compared with other groups. In addition, the grafted ADSCs could gain vascular endothelial-like phenotypes, which was in agreement with our previous research [28, 53], thereby further explaining why the 3D-bioprinted engineering ovary had more pronounced vascularization. Next, we further evaluated the effects of the novel 3D-bioprinted engineering ovary on restoration of ovarian function. We observed that the proportion of follicles at all development stages continued to increase significantly rather than only partially activation of growing follicles, which was considered to be associated with the early post-transplantation revascularization and the ADSCs’ capacity of selective activation of primordial follicles, and in turn improve protection of ovarian reserve. We also observed obviously increased ki67 staining and decreased caspase-3 staining of GCs after 3D-bioprinted engineering ovary transplantation, indicating that more retention ADSCs had better protective effects of GCs induced by CTX. Additionally, we examined the hormone levels to evaluate the restoration of hypothalamic-pituitary-ovarian (HPO) endocrine axis. The findings demonstrated significantly increased E2 and AMH levels as well as decreased FSH levels after transplantation of 3D-bioprinted engineering ovary, which corresponded with the increased number of GCs of follicles at all stages. The therapeutic

effect was also confirmed by the restoration of estrous cycle, which was another evaluation index for recovery of ovarian function. Taken together, these results verified that 3D-bioprinted engineering ovary transplantation resulted in better ovarian functional recovery than other treatment groups, which may provide a novel therapeutic strategy for POI patients.

Our above studies demonstrated that we successful reconstructed a 3D-bioprinted engineering ovary by remodeling of an early and long-term vascular system in the construct, which increased the survival of follicles and ovarian function. To further elucidate the mechanism responsible for angiogenesis, we detected the mRNA expression levels of angiogenic factors (eg. VEGF, FGF-2 and angiogenin)[54–56] in all groups. It was found that their mRNA expression levels in 3D-bioprinted engineering ovary were significantly higher than those in other groups, suggesting that the presence of rich vascular network in the construct was attributed to a high concentration of angiogenic factors induced by ADSCs. It is generally accepted that PI3K/AKT signaling pathway plays a crucial role in stimulating angiogenesis, activating primary follicles, and further reducing ovarian damage [38, 57, 58]. Our results revealed elevated PI3K, p-AKT, and VEGF levels in the fragment-cell group and 3D-bioprinted engineering ovary group, especially the latter one, suggesting that the activation of PI3K/AKT signaling pathway might be involved in the regulation of ADSCs' effects on angiogenesis. Taken together, these studies indicated that transplantation of 3D-bioprinted engineering ovary promoted angiogenesis and restored ovarian functions through the PI3K/AKT signaling pathway.

The 3D-bioprinted engineering ovary developed in this study is a critical first step to evaluate the effectiveness of exploring such a method for restoring ovarian function in POI. Our further study will focus on improvement of 3D-bioprinted scaffold for orthotropic ovary transplantation and thus assessment of the efficiency of fertility improvement. In this study, we investigated the effectiveness of ADSCs in protecting ovarian reserve and regulating angiogenesis, but failed to ascertain whether this method could improve quality of oocytes. It is, therefore, a series of relevant experiments will be performed in our follow-up studies. In our study, we successful removed grafts and found excellent biocompatibility between scaffold and ovarian tissues; however, inflammation-based indicators in serum and grafts were not detected in our study, which need further additional exploration. With preliminary study presented here, more animals and extended observed time are needed in our future studies to provide sufficient supporting evidence for future clinical studies.

Excitingly, 3D-bioprinted engineering ovary transplantation is indeed showing great potential for restoring impaired ovarian function in POI. Our results are encouraging, although clinical applications still have a long way to go. Our studies clearly demonstrated that 3D-bioprinted ADSCs-loaded scaffold constructed a higher rate of vascularization and reduced massive follicle loss in the early grafting period, which could compensate for the disadvantages of IVA to some extent. Moreover, our findings raise the possibility that the 3D-bioprinted ADSCs-loaded scaffold may provide an effective method for cryopreserved ovarian tissue grafting.

Conclusion

In conclusion, we have demonstrated that 3D-bioprinted scaffold could improve retention of ADSCs and revascularization in the grafts. In addition, we designed for the first time that a 3D-bioprinted engineering ovary composed of IVA and ADSCs, which contributed to a more effective approach to restoration of ovarian function in POI rats.

Abbreviations

Drug-free IVA
Drug-free in vitro activation
POI
Premature ovarian insufficiency
MSCs
Mesenchymal stem cells
ADSCs
Adipose-derived stem cells
PTEN
Phosphatase and tensin homolog
PI3K
Phosphatidylinositol-3-kinase
AKT
Protein kinase B
FOXO3
Forkhead box O3
GCs
Granulosa cells
dECM
Decellularized extracellular matrix
FCM
Flow cytometry
HE
Hematoxylin and eosin
DAPI
4’6-Diamidino-2-Phenylindole
PBS
Phosphate-buffered saline
CTX
Cyclophosphamide
OCT
Optimal cutting temperature
IF

Immunofluorescence
ELISA
Enzyme-linked immunosorbent assay
E2
Estradiol
FSH
Follicle stimulating hormone
AMH
Antimüllerian hormone
BSA
Bovine serum albumin
cDNA
Complementary DNA.

Declarations

Ethics approval and consent to participate

The study was approved by the Ethics Committee of Second Hospital of Hebei Medical University (2021-AE055). All animal experiments were performed in accordance with the ethical guidelines approved by the Animal Care and Research Committee of Hebei University.

Consent for publication

Not applicable.

Competing interests

All authors declare that they have no conflict of interests.

Fundings

This study was supported by the Natural Precision Medicine Joint Fund Nurture Project of Hebei Province (H2021206463); the Medical Science Research Plan Project of Hebei Province (20210080); the Innovative Capacity Improvement Plan Of Hebei Province (20577705D).

Authors’ contributions

Q.L., X.H.H. and J.K.Z. conceived and designed the study. Q.L., J.H.Z. and J.K.Z. performed the experiments and drafted the manuscript. Q.L., J.H.Z. and Z.K.L. participated in data analysis and made the figures in this manuscript. Y.L.X., M.L.Z., W.X.S. and H.G. participated in the discussion and revised

the manuscript. X.H.H., J.K.Z. and Q.L. were responsible for the critical review of the manuscript. All authors contributed to this work, discussed the results, critically reviewed and revised the manuscript. All authors read and approved the final manuscript.

Acknowledgements

The authors would like to thank Dr. Yanbiao Song for his technical assistance.

References

1. Kovanci E, Schutt AK. Premature ovarian failure: clinical presentation and treatment. Obstet Gynecol Clin North Am. 2015;42(1):153 – 61. https://doi.org/10.1016/j.ogc.2014.10.004.
2. Kawamura K, Kawamura N, Hsueh AJ. Activation of dormant follicles: a new treatment for premature ovarian failure? Curr Opin Obstet Gynecol. 2016;28(3):217–22. https//doi.org/10.1097/GCO.0000000000000268.
3. Kawamura K, Cheng Y, Suzuki N, Deguchi M, Sato Y, e a Takae S. Hippo signaling disruptionand Akt stimulation of ovarian follicles for infertility treatment. Proc Natl Acad Sci USA. 2013;110(43):17474–9. https//doi.org/10.1073/pnas.1312830110.
4. Grosbois J, Demeestere I. Dynamics of PI3K and Hippo signaling pathways during in vitro human follicle activation. Hum Reprod. 2018;33(9):1705–14. https//doi.org/10.1093/humrep/dey250.
5. Maidarti M, Anderson RA, Telfer EE. Crosstalk between PTEN/PI3K/Akt Signalling and DNA Damage in the Oocyte: Implications for Primordial Follicle Activation, Oocyte Quality and Ageing. Cells. 2020;9(1):200. https//doi.org/10.3390/cells9010200.
6. Fabregues F, Ferreri J, Calafell JM, Moreno V, Borrás A, Manau D, Carmona F. Pregnancy after drug-free in vitro activation of follicles and fresh tissue autotransplantation in primary ovarian insufficiency patient: a case report and literature review. J Ovarian Res. 2018;11(1):76. https//doi.org/10.1186/s13048-018-0447-3.
7. Ferreri J, Fabregues F, Calafell JM, Solernou R, Borras A, Saco A, Manau D, Carmona F. Drug-free in-vitro activation of follicles and fresh tissue autotransplantation as a therapeutic option in patients with primary ovarian insufficiency. Reprod Biomed Online. 2020;40(2):254–60. https//doi.org/10.1016/j.rbmo.2019.11.009.
8. Kazuhiro K, Bunpei I, Hsueh AJW. Drug-free in-vitro activation of follicles for infertility treatment in poor ovarian response patients with decreased ovarian reserve. Reprod Biomed Online. 2020;40(2):245–53. https//doi.org/10.1016/j.rbmo.2019.09.007.
9. Lunding SA, Pors SE, Kristensen SG, Landersoe SK, Jeppesen JV, Flachs EM, Pinborg A, Macklon KT, Pedersen AT, Andersen CY. A N Andersen. Biopsying, fragmentation and autotransplantation of fresh ovarian cortical tissue in infertile women with diminished ovarian reserve. Hum Reprod. 2019;34(10):1924–36. https//doi.org/10.1093/humrep/dez152.

10. Suzuki N, Yoshioka N, Takae S, Sugishita Y, Tamura M, Hashimoto S, Morimoto Y, Kawamura K. Successful fertility preservation following ovarian tissue vitrification in patients with primary ovarian insufficiency. Hum Reprod. 2015;30(3):608–15. https//doi.org/10.1093/humrep/deu353.
11. Zhai J, Yao G, Dong F, Bu Z, Cheng Y, Sato Y, Hu L, Zhang Y, Wang J, Dai S, Li J, Sun J, Hsueh AJ, Kawamura K. Y Sun. In Vitro Activation of Follicles and Fresh Tissue Auto-transplantation in Primary Ovarian Insufficiency Patients. J Clin Endocrinol Metab. 2016;101(11):4405–12. https//doi.org/10.1210/jc.2016-1589.
12. Zhang X, Han T, Yan L, Jiao X, Qin Y, Chen ZJ. Resumption of Ovarian Function After Ovarian Biopsy/Scratch in Patients With Premature Ovarian Insufficiency. Reprod Sci. 2019;26(2):207–13. https//doi.org/10.1177/1933719118818906.
13. Wang W, Todorov P, Isachenko E, Rahimi G, Mallmann P, Wang M, Isachenko V. In vitro activation of cryopreserved ovarian tissue: A single-arm meta-analysis and systematic review. Eur J Obstet Gynecol Reprod Biol. 2021;258(2021):258–64. https//doi.org/10.1016/j.ejogrb.2021.01.014.
14. Masciangelo R, Hossay C, Chiti MC, Manavella DD, Amorim CA, Donnez J, Dolmans MM. Role of the PI3K and Hippo pathways in follicle activation after grafting of human ovarian tissue. J Assist Reprod Genet. 2020;37(1):101–08. https//doi.org/10.1007/s10815-019-01628-1.
15. Xia X, Yin T, Yan J, Yan L, Jin C, Lu C, Wang T, Zhu X, Zhi X, Wang J, Tian L, Liu J, Li R. J Qiao. Mesenchymal Stem Cells Enhance Angiogenesis and Follicle Survival in Human Cryopreserved Ovarian Cortex Transplantation. Cell Transpl. 2015;24(10):1999–2010. https//doi.org/10.3727/096368914X685267.
16. Zhang Y, Xia X, Yan J, Yan L, Lu C, Zhu X, Wang T, Yin T, Li R, Chang HM, Qiao J. Mesenchymal stem cell-derived angiogenin promotes primodial follicle survival and angiogenesis in transplanted human ovarian tissue. Reprod Biol Endocrinol. 2017;15(1):18. https//doi.org/10.1186/s12958-017-0235-8.
17. Ding C, Zou Q, Wang F, Wu H, Chen R, Lv J, Ling M, Sun J, Wang W, Li H, Huang B. Human amniotic mesenchymal stem cells improve ovarian function in natural aging through secreting hepatocyte growth factor and epidermal growth factor. Stem Cell Res Ther. 2018;9(1):55. https//doi.org/10.1186/s13287-018-0781-9.
18. Li J, Mao Q, He J, She H, Zhang Z, Yin C. Human umbilical cord mesenchymal stem cells improve the reserve function of perimenopausal ovary via a paracrine mechanism. Stem Cell Res Ther. 2017;8(1):55. https//doi.org/10.1186/s13287-017-0514-5.
19. Liu H, Jiang C, La B, Cao M, Ning S, Zhou J, Yan Z, Li C, Cui Y, Ma X, Wang M, Chen L, Yu Y, Chen F, Zhang Y, Wu H, Liu J, Qin L. Human amnion-derived mesenchymal stem cells improved the reproductive function of age-related diminished ovarian reserve in mice through Ampk/FoxO3a signaling pathway. Stem Cell Res Ther. 2021;12(1):317. https//doi.org/10.1186/s13287-021-02382-x.
20. Suuronen EJ, Veinot JP, Wong S, Kapila V, Price J, Griffith M, Mesana TG, Ruel M. Tissue-engineered injectable collagen-based matrices for improved cell delivery and vascularization of ischemic tissue

using CD133 + progenitors expanded from the peripheral blood. Circulation. 2006;114(1 Suppl):I138-44. https//doi.org/10.1161/CIRCULATIONAHA.105.001081.

21. Ding L, Yan G, Wang B, Xu L, Gu Y, Ru T, Cui X, Lei L, Liu J, Sheng X, Wang B, Zhang C, Yang Y, Jiang R, Zhou J, Kong N, Lu F, Zhou H, Zhao Y, Chen B, Hu Y, Dai J. H Sun. Transplantation of UC-MSCs on collagen scaffold activates follicles in dormant ovaries of POF patients with long history of infertility. Sci China Life Sci. 2018;61(12):1554–65. https//doi.org/10.1007/s11427-017-9272-2.
22. Su J, Ding L, Cheng J, Yang J, Li X, Yan G, Sun H, Dai J, Hu Y. Transplantation of adipose-derived stem cells combined with collagen scaffolds restores ovarian function in a rat model of premature ovarian insufficiency. Hum Reprod. 2016;31(5):1075–86. https//doi.org/10.1093/humrep/dew041.
23. Badylak SF, Freytes DO, Gilbert TW. Reprint of: Extracellular matrix as a biological scaffold material: Structure and function. Acta Biomater. 2015;23:upplS17–26. https//doi.org/10.1016/j.actbio.2015.07.016.
24. Jakus AE, Laronda MM, Rashedi AS, Robinson CM, Lee C, Jordan SW, Orwig KE, Woodruff TK, Shah RN. “Tissue Papers” from Organ-Specific Decellularized Extracellular Matrices. Adv Funct Mater. 2017;27(34):1700992. https//doi.org/10.1002/adfm.201700992.
25. Pennarossa G, Arcuri S, De Iorio T, Gandolfi F. T A L Brevini. Current Advances in 3D Tissue and Organ Reconstruction. Int J Mol Sci. 2021;22(2):830. https//doi.org/10.3390/ijms22020830.
26. Zuk PA, Zhu M, Ashjian P, De Ugarte DA, Huang JI, Mizuno H, Alfonso ZC, Fraser JK, Benhaim P, Hedrick MH. Human adipose tissue is a source of multipotent stem cells. Mol Biol Cell. 2002;13(12):4279–95. https//doi.org/10.1091/mbc.e02-02-0105.
27. Zhang JK, Du RX, Zhang L, Li YN, Zhang ML, Zhao S, Huang XH, Xu YF. A new material for tissue engineered vagina reconstruction: Acellular porcine vagina matrix. J Biomed Mater Res A. 2017;105(7):1949–59. https//doi.org/10.1002/jbm.a.36066.
28. Hou C, Zheng J, Li Z, Qi X, Tian Y, Zhang M, Zhang J, Huang X. Printing 3D vagina tissue analogues with vagina decellularized extracellular matrix bioink. Int J Biol Macromol. 2021;180(2021):177–86. https//doi.org/10.1016/j.ijbiomac.2021.03.070.
29. Ling L, Feng X, Wei T, Wang Y, Wang Y, Wang Z, Tang D, Luo Y, Xiong Z. Human amnion-derived mesenchymal stem cell (hAD-MSC) transplantation improves ovarian function in rats with premature ovarian insufficiency (POI) at least partly through a paracrine mechanism. Stem Cell Res Ther. 2019;10(1):46. https//doi.org/10.1186/s13287-019-1136-x.
30. Li Z, Zhang M, Zheng J, Tian Y, Zhang H, Tan Y, Li Q, Zhang J, Huang X. Human Umbilical Cord Mesenchymal Stem Cell-Derived Exosomes Improve Ovarian Function and Proliferation of Premature Ovarian Insufficiency by Regulating the Hippo Signaling Pathway. Front Endocrinol (Lausanne). 2021;12711902. https//doi.org/10.3389/fendo.2021.711902.
31. Zhao S, Qi W, Zheng J, Tian Y, Qi X, Kong D, Zhang J, Huang X. Exosomes Derived from Adipose Mesenchymal Stem Cells Restore Functional Endometrium in a Rat Model of Intrauterine Adhesions. Reprod Sci. 2020;27(6):1266–75. https//doi.org/10.1007/s43032-019-00112-6.

32. Badylak SF. Xenogeneic extracellular matrix as a scaffold for tissue reconstruction. Transpl Immunol. 2004;12(3–4):367–77. https//doi.org/10.1016/j.trim.2003.12.016.
33. Uygun BE, Soto-Gutierrez A, Yagi H, Izamis ML, Guzzardi MA, Shulman C, Milwid J, Kobayashi N, Tilles A, Berthiaume F, Hertl M, Nahmias Y, Yarmush ML, Uygun K. Organ reengineering through development of a transplantable recellularized liver graft using decellularized liver matrix. Nat Med. 2010;16(7):814–20. https//doi.org/10.1038/nm.2170.
34. Van Eyck AS, Jordan BF, Gallez B, Heilier JF, Van Langendonckt A, Donnez J. Electron paramagnetic resonance as a tool to evaluate human ovarian tissue reoxygenation after xenografting. Fertil Steril. 2009;92(1):374–81. https//doi.org/10.1016/j.fertnstert.2008.05.012.
35. Mahmoodi M, Soleimani Mehranjani M, Shariatzadeh SM, Eimani H, Shahverdi A. Effects of erythropoietin on ischemia, follicular survival, and ovarian function in ovarian grafts. Reproduction. 2014;147(5):733–41. https//doi.org/10.1530/REP-13-0379.
36. Mahmoodi M, Soleimani Mehranjani M, Shariatzadeh SM, Eimani H, Shahverdi A. N-acetylcysteine improves function and follicular survival in mice ovarian grafts through inhibition of oxidative stress. Reprod Biomed Online. 2015;30(1):101–10. https//doi.org/10.1016/j.rbmo.2014.09.013.
37. Lai D, Wang F, Yao X, Zhang Q, Wu X, Xiang C. Human endometrial mesenchymal stem cells restore ovarian function through improving the renewal of germline stem cells in a mouse model of premature ovarian failure. J Transl Med. 2015;13:155. https//doi.org/10.1186/s12967-015-0516-y.
38. Yang Z, Du X, Wang C, Zhang J, Liu C, Li Y, Jiang H. Therapeutic effects of human umbilical cord mesenchymal stem cell-derived microvesicles on premature ovarian insufficiency in mice. Stem Cell Res Ther. 2019;10(1):250. https//doi.org/10.1186/s13287-019-1327-5.
39. Liu R, Zhang X, Fan Z, Wang Y, Yao G, Wan X, Liu Z, Yang B, Yu L. Human amniotic mesenchymal stem cells improve the follicular microenvironment to recover ovarian function in premature ovarian failure mice. Stem Cell Res Ther. 2019;10(1):299. https//doi.org/10.1186/s13287-019-1315-9.
40. Lafosse A, Desmet C, Aouassar N, Andre W, Hanet MS, Beauloye C, Vanwijck R, Poirel HA, Gallez B. D Dufrane. Autologous Adipose Stromal Cells Seeded onto a Human Collagen Matrix for Dermal Regeneration in Chronic Wounds: Clinical Proof of Concept. Plast Reconstr Surg. 2015;136(2):279–95. https//doi.org/10.1097/PRS.0000000000001437.
41. Manavella DD, Cacciottola L, Desmet CM, Jordan BF, Donnez J, Amorim CA, Dolmans MM. Adipose tissue-derived stem cells in a fibrin implant enhance neovascularization in a peritoneal grafting site: a potential way to improve ovarian tissue transplantation. Hum Reprod. 2018;33(2):270–79. https//doi.org/10.1093/humrep/dex374.
42. Manavella DD, Cacciottola L, Pomme S, Desmet CM, Jordan BF, Donnez J, Amorim CA, Dolmans MM. Two-step transplantation with adipose tissue-derived stem cells increases follicle survival by enhancing vascularization in xenografted frozen-thawed human ovarian tissue. Hum Reprod. 2018;33(6):1107–16. https//doi.org/10.1093/humrep/dey080.
43. Yang W, Zhang J, Xu B, He Y, Liu W, Li J, Zhang S, Lin X, Su D, Wu T, Li J. HucMSC-Derived Exosomes Mitigate the Age-Related Retardation of Fertility in Female Mice. Mol Ther. 2020;28(4):1200–13.

https//doi.org/10.1016/j.ymthe.2020.02.003.

44. Sun M, Wang S, Li Y, Yu L, Gu F, Wang C. Y Y. Adipose-derived stem cells improved mouse ovary function after chemotherapy-induced ovary failure. Stem Cell Res Ther. 2013;4(4):80. https://doi.org/10.1186/scrt231.
45. Smets FN, Chen Y, Wang LJ. S HE. Loss of cell anchorage triggers apoptosis (anoikis) in primary mouse hepatocyte. Mol Genet Metab. 2002;75(4):344–52. https://doi.org/10.1016/S1096-7192(02)00004-5.
46. Kim J, Perez AS, Claflin J, David A, Zhou H, Shikanov A. Synthetic hydrogel supports the function and regeneration of artificial ovarian tissue in mice. NPJ Regen Med. 2016;1:16010. https://doi.org/10.1038/npjregenmed.2016.10.
47. Yang Y, Lei L, Wang S, Sheng X, Yan G, Xu L, Liu J, Liu M, Zhen X, Ding L, Sun H. Transplantation of umbilical cord-derived mesenchymal stem cells on a collagen scaffold improves ovarian function in a premature ovarian failure model of mice. In Vitro Cell Dev Biol Anim. 2019;55(4):302–11. https://doi.org/10.1007/s11626-019-00337-4.
48. Kim BS, Das S, Jang J, Cho D-W. Decellularized Extracellular Matrix-based Bioinks for Engineering Tissue- and Organ-specific Microenvironments. Chem Rev. 2020;120(19):10608–61. https://doi.org/10.1021/acs.chemrev.9b00808.
49. Choudhury D, Tun HW, Wang T, Naing MW. Organ-Derived Decellularized Extracellular Matrix: A Game Changer for Bioink Manufacturing? Trends Biotechnol. 2018;36(8):787–805. https://doi.org/10.1016/j.tibtech.2018.03.003.
50. Pati F, Jang J, Ha D-H, Won Kim S, Rhie J-W, Shim J-H, Kim D-H, Cho D-W. Printing three-dimensional tissue analogues with decellularized extracellular matrix bioink. Nat Commun. 2014;5(1):3935. https://doi.org/10.1038/ncomms4935.
51. Abaci A, Guvendiren M. Designing Decellularized Extracellular Matrix-Based Bioinks for 3D Bioprinting. Adv Healthc Mater. 2020;9(24):e2000734. https://doi.org/10.1002/adhm.202000734.
52. Petersen TH, Calle EA, Zhao L, Lee EJ, Gui L, Raredon MB, Gavrilov K, Yi T, Zhuang ZW, Breuer C, Herzog E, Niklason LE. Tissue-engineered lungs for in vivo implantation. Science. 2010;329(5991):538–41. https://doi.org/10.1126/science.1189345.
53. Zhang H, Zhang J, Huang X, Li Y. The Methods and Mechanisms to Differentiate Endothelial-Like Cells and Smooth Muscle Cells from Mesenchymal Stem Cells for Vascularization in Vaginal Reconstruction. Mol Biotechnol. 2018;60(6):396–411. https://doi.org/10.1007/s12033-018-0079-2.
54. Mao J, Smith MF, Rucker EB, Wu GM, McCauley TC, Cantley TC, Prather RS, Didion BA. D BN. Effect of epidermal growth factor and insulin-like growth factor I on reantral follicular growth, antrum formation, and stimulation of granulosal cell porcine proliferation and suppression of apoptosis in vitro. J Anim Sci. 2004;82(7):1967–75. https://doi.org/10.2527/2004.8271967x.
55. Sharma GT, Dubey PK, Kumar GS. Effects of IGF-1, TGF-alpha plus TGF-beta1 and bFGF on in vitro survival, growth and apoptosis in FSH-stimulated buffalo (Bubalis bubalus) preantral follicles. Growth Horm IGF Res. 2010;20(4):319–25. https://doi.org/10.1016/j.ghir.2010.05.001.

56. Shin SY, Lee JY, Lee E, Choi J, Yoon BK, Bae D, Choi D. Protective effect of vascular endothelial growth factor (VEGF) in frozen-thawed granulosa cells is mediated by inhibition of apoptosis. Eur J Obstet Gynecol Reprod Biol. 2006;125(2):233–8. https://doi.org/10.1016/j.ejogrb.2005.10.027.
57. Takahashi A, Yousif A, Hong L, Chefetz I. Premature ovarian insufficiency: pathogenesis and therapeutic potential of mesenchymal stem cell. J Mol Med. 2021;99(5):637–50. https://doi.org/10.1007/s00109-021-02055-5.
58. Hung SC, Pochampally RR, Chen SC, Hsu SC, Prockop DJ. Angiogenic effects of human multipotent stromal cell conditioned medium activate the PI3K-Akt pathway in hypoxic endothelial cells to inhibit apoptosis, increase survival, and stimulate angiogenesis. Stem Cells. 2007;25(9):2363–70. https://doi.org/10.1634/stemcells.2006-0686.

Figures

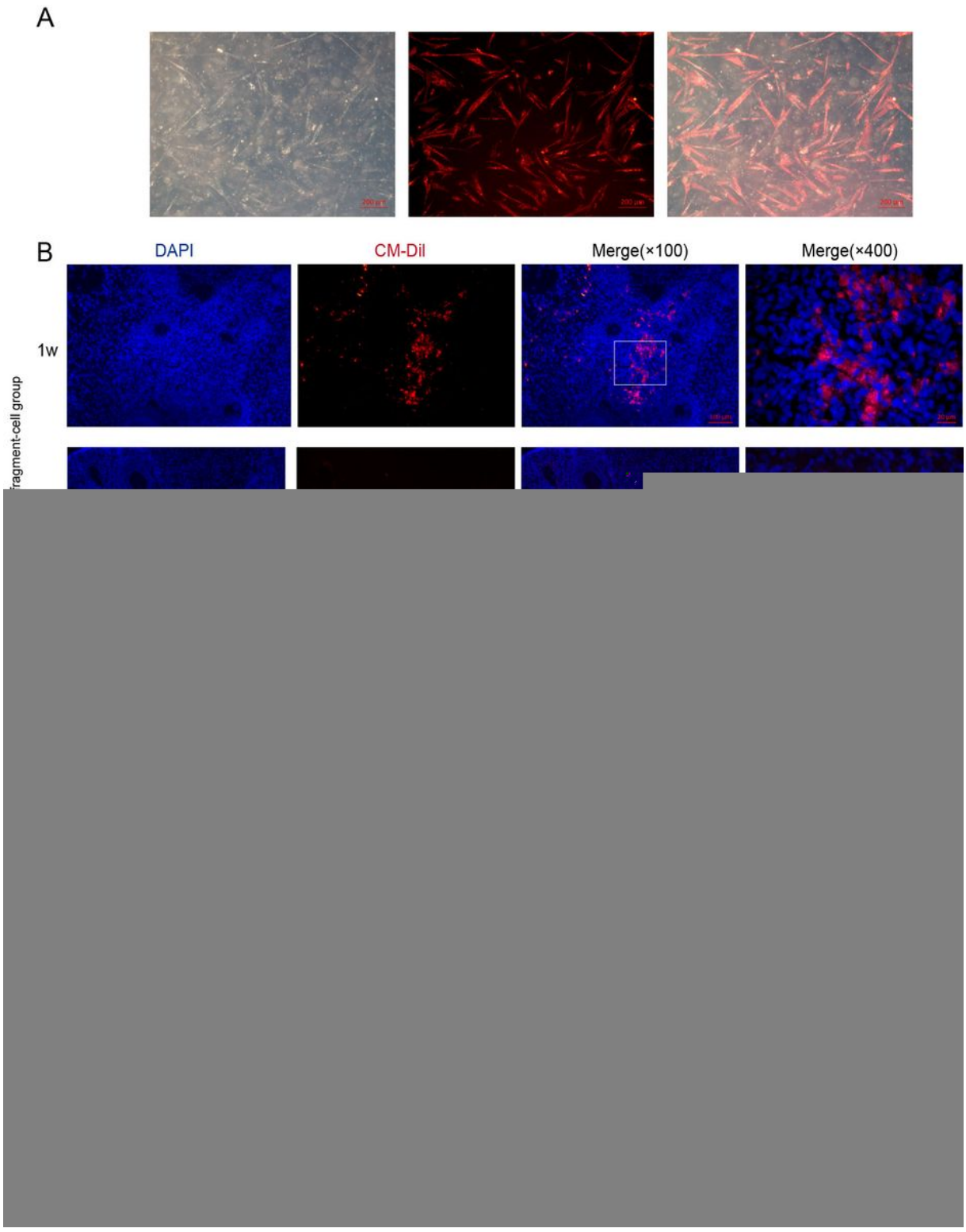

Figure 1

Localization and differentiation of ADSCs in grafts. (A) CM-Dil stained ADSCs showed red fluorescence in vitro. Scale bar: 200um. (B) Localization of CM-Dil stained ADSCs in the fragment-cell group and 3D-bioprinted engineering ovary group at 1 week and 4 weeks after transplantation. ADSCs mainly distributed in interstitium of ovarian and progressively reduced over time, but the 3D-bioprinted engineering ovary group had higher retention ratio of ADSCs. Scale bar: 100um and 20um. (C) CM-Dil

stained ADSCs (red) was co-localized with CD31 staining (green) in vascular endothelial cells of 3D-bioprinted engineering ovary group after 4 weeks transplantation. Scale bar: 50um.

Figure 2

Profiles of grafts pre- and post-transplantation. (A) Schematic representation of construction of 3D-bioprinted engineering ovary. (B) Photographs of 3D-bioprinted engineering ovary group related to surgical procedure, including preparing 3D scaffolds (a) and POI ovarian cortex fragments (b), wrapping ovarian fragments into 3D scaffolds (c) and subcutaneous transplanting (d). (C) Macroscopic evaluation of grafts after 2 and 4 weeks transplantation. The ovarian fragments (with or without ADSCs) could rejoin and wrap by a hyaline membrane (a, b, c, d) and 3D constructs could maintain their structure (e, f, g, h), all grafts were surrounded by visible functional blood vessels (black arrow), but the 3D-bioprinted engineering ovary grafts were more marked and had preovulatory follicles (h, i, white arrow).

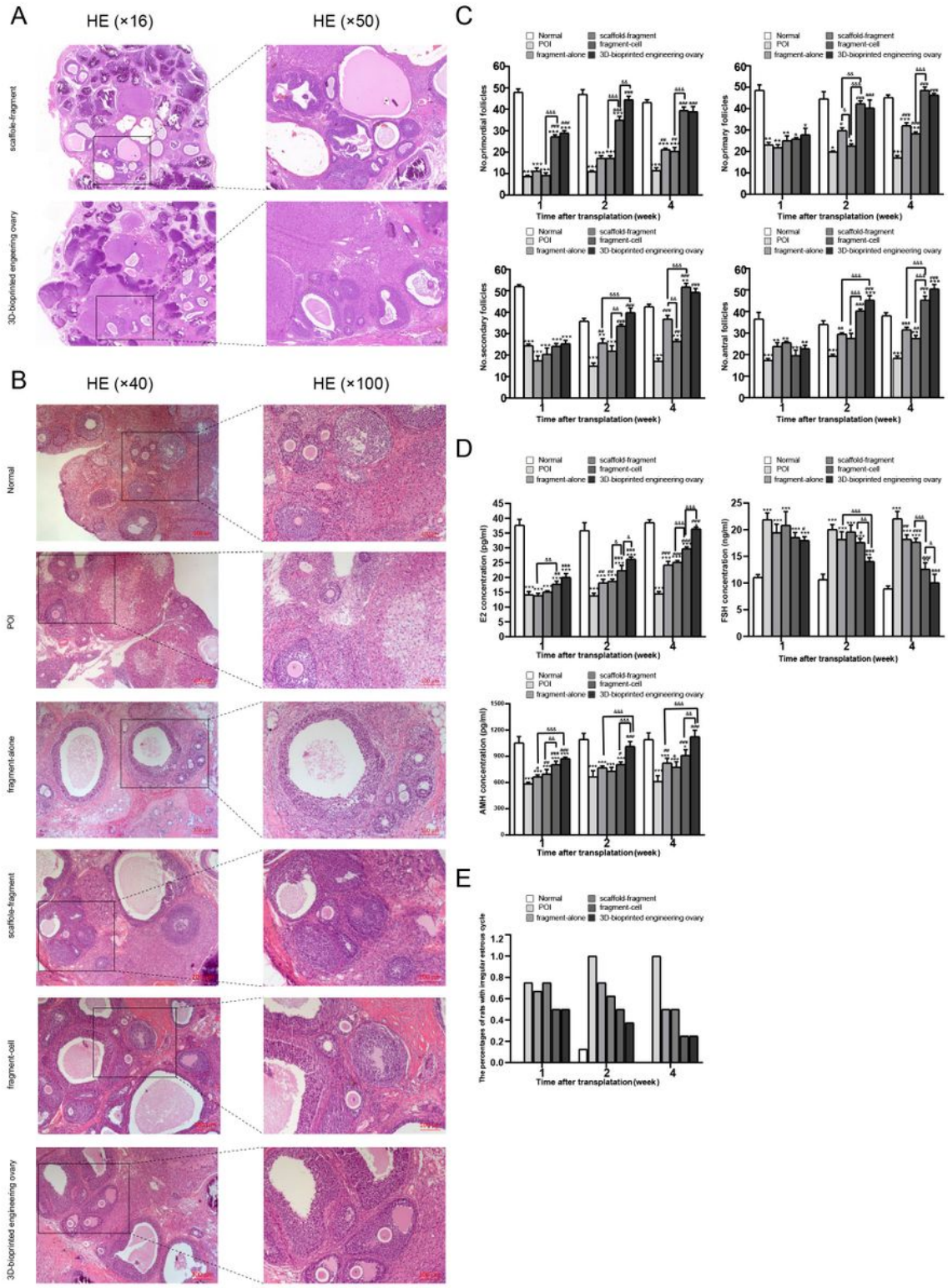

Figure 3

Ovarian functions after grafts transplantation. (A) Histological analysis of biocompatibility between ovarian tissue and 3D scaffold with/without ADSCs. Scale bar: 500um and 200um. (B) Histological analysis of ovaries in six different groups. Scale bar: 200um and 100um. (C) Number of follicles in different stages counted at 1, 2, and 4 weeks after grafts transplantation. (D) The levels of E2, FSH, and AMH were analyzed at 1, 2, and 4 weeks after grafts transplantation. (* vs the normal group, # vs the POI

group, & compare between two groups; *, #, & P<0.05; **, ##, && P<0.01; ***, ###, &&& P<0.005). (F) Changes of irregular estrous cycles.

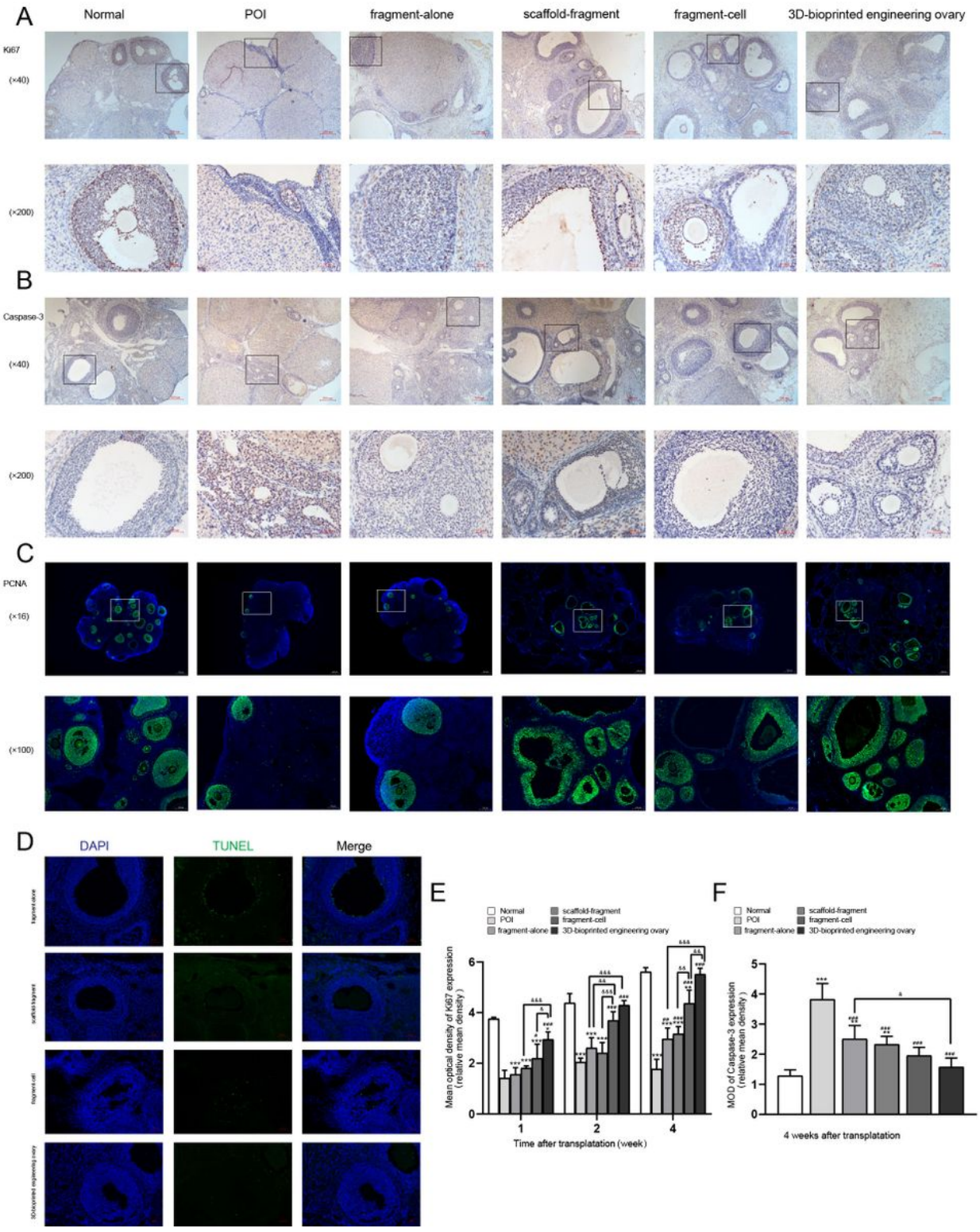

Figure 4

Proliferation and apoptosis of granulosa cells (GCs) after grafts transplantation. Representative immunohistochemical images of Ki67 (A) and Casepase-3 (B) in six different groups. Scale bar: 50um

and 200um. (C) Representative immunofluorescence staining of PCNA in six different groups. Scale bar: 500um and 100um. (D) Representative pictures of TUNEL staining from the four treatment groups. Green staining represents apoptotic GCs. Scale bar: 50um. The mean optical density (MOD) of ki67-positive (E) and casepase-3-positive areas (F) were analyzed by Image-Pro Plus. (* vs the normal group, # vs the POI group, & compare between two groups; *, #, & P<0.05; **, ##, && P<0.01; ***, ###, &&& P <0.005).

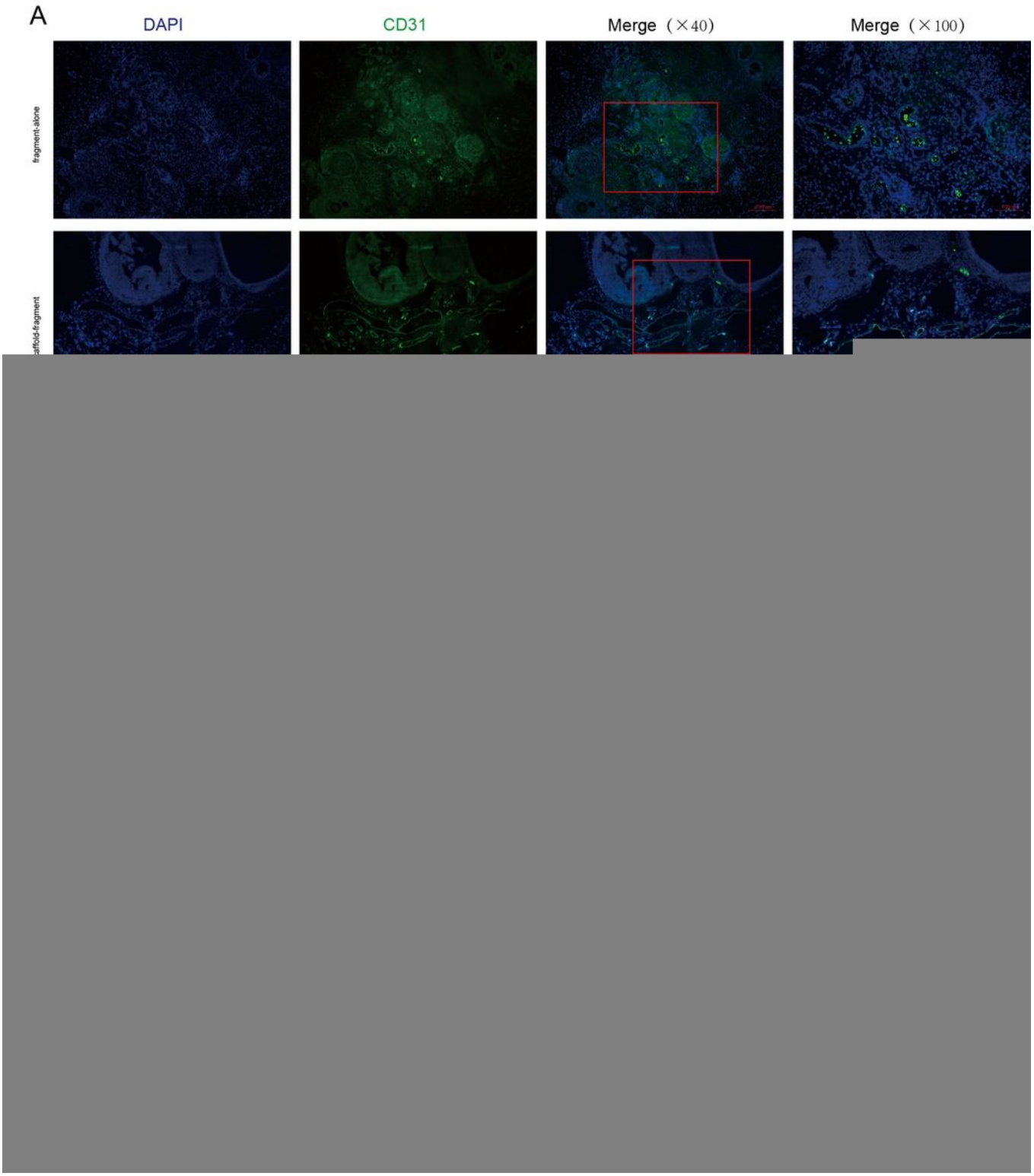

Figure 5

Assessment of grafts revascularization. (A) Angiogenesis shown in representative images of CD31-positve vessels in fragment-alone group, scaffold-fragment group, fragment-cell group, 3D-bioprinted engineering ovary group at 1 week after grafts transplantation. Scale bar: 200um and 100um. (B) Data analysis of blood vessels density (number of blood vessels (nb) per mm^2) was performed in four treatment groups at 1 week and 4 weeks after transplantation. The significantly higher vessels density in 3D-bioprinted engineering ovary group from 1 week to 4 weeks post-transplantation, indicated the more progressed and continuous vascular remodeling. (* P<0.05, ** P <0.01, *** P <0.005).

Figure 6

Promoted angiogenesis by regulating PI3K/AKT pathway and secreting proangiogenic factors. (A) Representative PI3K, p-AKT, AKT and VEGF bands of PI3K/AKT pathway using GAPDH as the internal reference. (B) Quantitative analysis of protein expression shown that the expression level of PI3K, p-AKT and VEGF was increased in fragment-cell group and 3D-bioprinted engineering ovary group, while the level of AKT did not show significant difference in the groups. (C) The mRNA levels of VEGF, FGF-2, and angiogenin were upregulated in the 3D-bioprinted engineering ovary group. (* vs the normal group, # vs the POI group, & compare between two groups; *, #, & P<0.05; **, ##, && P<0.01; ***, ###, &&& P <0.005).

Supplementary Files

This is a list of supplementary files associated with this preprint. Click to download.

- figureS1.tif
- figureS2.tif